

# Giant momentum-dependent spin splitting in symmetric low Z antiferromagnets

Lin-Ding Yuan<sup>1</sup>, Zhi Wang<sup>1\*</sup>, Jun-Wei Luo<sup>2</sup>, Emmanuel I. Rashba<sup>3\*</sup>, Alex Zunger<sup>1\*</sup>

The energy vs. crystal momentum  $E(k)$  diagram for a solid (band structure) constitutes the road map for navigating its optical, magnetic, and transport properties. By selecting crystals with specific atom types, composition and symmetries, one could design a target band structure and thus desired properties. A particularly attractive outcome would be to design energy bands that are split into spin components with a momentum-dependent splitting, enabling spintronic application. The current paper provides design principles for wavevector dependent spin splitting (SS) of energy bands<sup>1</sup> that parallels the traditional Dresselhaus<sup>2</sup> and Rashba<sup>3</sup> spin-orbit coupling (SOC) -induced splitting, but originates from a fundamentally different source—antiferromagnetism. We identify a few generic AFM prototypes with distinct SS patterns using magnetic symmetry design principles. These tools allow also the identification of specific AFM compounds with SS belonging to different prototypes. A specific compound-- centrosymmetric tetragonal  $\text{MnF}_2$ -- is used via density functional band structure calculations to quantitatively illustrate one type of AFM SS. Unlike the traditional SOC-induced effects<sup>2,3</sup> restricted to non- centrosymmetric crystals, we show that antiferromagnetic-induced spin splitting broadens the playing field to include even centrosymmetric compounds, and gives SS comparable in magnitude to the best known ('giant') SOC effects, even without SOC, and consequently does not rely on the often-unstable high atomic number elements required for high SOC. We envision that use of the current design principles to identify an optimal antiferromagnet with spin-split energy bands would be beneficial for efficient spin-charge conversion and spin orbit torque applications without the burden of requiring compounds containing heavy elements.

---

Emails: [erashba@physics.harvard.edu](mailto:erashba@physics.harvard.edu) ; [alex.zunger@colorado.edu](mailto:alex.zunger@colorado.edu)

Corresponding authors: Alex Zunger, Zhi Wang

<sup>1</sup>Energy Institute, University of Colorado, Boulder, CO 80309, USA

<sup>2</sup>State Key Laboratory for Superlattices and Microstructures, Institute of Semiconductors, Chinese Academy of Sciences, Beijing 100083, China.

<sup>3</sup>Department of Physics Harvard University, Cambridge, Massachusetts 02138, USA

An electron with momentum  $\mathbf{p}$  and mass  $m$  moving in an inversion symmetry-breaking electric field  $\mathbf{E}$  in a solid experiences an effective magnetic field  $\mathbf{B}_{\text{eff}} \sim \mathbf{E} \times \mathbf{p}/mc^2$  in its rest-frame, where  $c$  is the speed of light. In bulk crystals<sup>2</sup> this symmetry breaking electric field is given by the gradient of the crystal potential  $\mathbf{E} = -\nabla V$ , whereas in heterostructures<sup>3</sup> it can be produced by interfacial asymmetry, and in centrosymmetric compounds by the local asymmetry of individual structural sectors<sup>4</sup>. This intrinsic magnetic field couples the electron momentum to its spin, a relativistic effect leading to spin-orbit-coupling (SOC) induced spin splitting of energy bands at wave vectors differing from the time reversal invariant moments (TRIM). In the semi-relativistic Pauli equation, the SOC is described by the Thomas (T)<sup>5</sup> term  $H_T = -\frac{e\hbar}{4m^2c^2}[\boldsymbol{\sigma} \cdot (\nabla V(\mathbf{r}) \times \mathbf{p})]$  that couples electron spin  $\boldsymbol{\sigma}$  to its coordinate  $\mathbf{r}$  and momentum  $\mathbf{p}$ , and its fully relativistic generalization. These seminal studies have formed the basis for the development of spintronics<sup>6-8</sup>, bringing  $\mathbf{k}$ -dependent spin-orbit interaction to the forefront of solid-state physics, including applications to spin transistor, spin-orbit torque, spin Hall effect, topological insulators, and Majorana Fermions (see review in Ref. <sup>9</sup>). Since the relativistic spin-orbit interaction increases rapidly with atomic number  $Z$ , and since the strength of chemical bonds in compounds decreases rapidly with increasing atomic number<sup>10</sup>, the ease of breaking such fragile bonds-- creating free-carrier generating metal vacancies-- has been an unwelcome but constant companion of high SOC compounds both for spin splitting and for topological insulators applications.<sup>11-14</sup> This double limitation to high- $Z$  and non-centrosymmetric compounds has raised hopes for an alternative spin splitting mechanism in thermodynamically stable, low  $Z$  compounds of more general symmetries.

A phenomenological theory of magnetic spin splitting has been proposed 1964 by Pekar and Rashba <sup>1</sup>, suggesting that the presence in magnetic compounds of a spatially -dependent intrinsic magnetic field  $\mathbf{h}(\mathbf{r})$ , periodic with the crystal period, can lead to coupling of Pauli matrices  $\boldsymbol{\sigma}$  to this  $\mathbf{h}(\mathbf{r})$ . This would result in a magnetic mechanism of  $\mathbf{k}$ -dependent spin splitting, suggestive of a new type of spin orbit coupling. In terms of the relativistic expansion in  $1/c$ , this magnetic mechanism is of the same order  $1/c^2$  as the Thomas term because both the Bohr magneton  $\mu_B = e\hbar/2mc$  and the field  $\mathbf{h}(\mathbf{r})$  produced by electron magnetization are of the order of  $1/c$ . Because the  $\mathbf{k} \cdot \mathbf{p}$  formalism used in Ref. <sup>1</sup> did not afford an atomistic definition of  $\mathbf{h}(\mathbf{r})$  and its ensuing spin splitting, nor did it provide for guiding principles to select a target material for investigating such effects, examination of these 1964 ideas remained dormant for a long time.

More recently, the investigation of spin splitting of energy bands has been expanded to include in addition to non-magnetic (NM)<sup>15</sup> and ferromagnetic (FM) systems, also antiferromagnetic (AFM) ones, in particular for eliminating stray fields around FM elements.<sup>16-19</sup> For example, half-metallic behavior, indicating the existence of spin splitting has been noted in some AFM compounds<sup>20-22</sup>, but such occurrences were not a spin-splitting mechanism that is distinct from the traditional spin orbit effect<sup>2,3</sup>. (see supplementary section I for detail discussion of previous work on spin splitting in AFM) Indeed, it is generally implied that such splitting in the presence of background AFM may be treated just as SOC-induced splitting in NM materials<sup>2,3</sup>, through the same Thomas term<sup>5</sup>. For example, calculations on BiCoO<sub>3</sub> with SOC manifest a small change in its spin splitting due to its antiferromagnetism, and, as shown in Ref. <sup>23</sup>, if SOC is deliberately removed from the Hamiltonian, the system has vanishing spin splitting in the whole Brillouin Zone (BZ). Also, the field-free magnetic mechanism discussed in the

present paper differs from the anomalous spin-orbit coupling in antiferromagnets induced by applying external magnetic field, discussed in Ref. <sup>24,25</sup>.

In the present paper, inspired by Ref. <sup>1</sup>, we demonstrate an alternative mechanism to SOC that creates spin splitting  $\Delta_{ss}(\mathbf{k})$  even in centrosymmetric crystals, and even if SOC is deliberately removed from the Hamiltonian (i.e., corresponding to low Z compounds), persists even at time reversal invariant wave vectors, and has an unusual *quadratic* scaling on momentum  $\mathbf{k}$ . The coupling of spin to lattice via the periodic spatial dependent intrinsic magnetic field  $h(\mathbf{r})$  is analogous to a new form of spin orbit coupling; the fact that spin splitting can exist without the presence of spin orbit interaction in the Hamiltonian is noteworthy. We formulate the general fundamental magnetic space group conditions (“design principles”) for spin splitting that reveal a few different, generic AFM prototype behaviors. Such tools allow identification of specific AFM compounds belonging to such prototype behaviors. We describe the characteristic fingerprints of such spin splitting effects (dependence on SOC, spin texture types) that would aid its eventual experimental testing.

**Symmetries that enforce spin degeneracy:** To select a compound for direct magnetic  $\mathbf{k}$ -dependent spin splitting we inspect the underlying symmetry requirements. We first list the symmetries that *keep* spin degeneracy, preventing SS, then discuss how to violate those symmetries (i) As is known<sup>26</sup>, the combination  $\theta I$  of time reversal  $\theta$  and spatial inversion  $I$  symmetries ensures double degeneracy for arbitrary wave vector  $\mathbf{k}$ . Likewise, (ii) when SOC is turned off, the spin and spatial degrees of freedom are decoupled, so there could exist pure spin rotation  $U$ , a spinor symmetry, that reverses the spin but keeps momentum invariance, thus preserving spin degeneracy for all wave vectors. The spin rotation  $U$  does not exist in AFM when the alternating magnetic moments exist on different atomic sites, because such arrangement reverses the antiferromagnetic order. But in a specific types of AFM compound (referred to as magnetic space group (MSG) type IV, such as  $\text{BiCoO}_3$ <sup>23</sup>) where there exists a translation  $T$  that transforms the reversed antiferromagnetic order back,  $UT$  symmetry would still preserve spin degeneracy for all wave vectors.

**Violating degeneracy-enforcing symmetries:** (i) As expected, the appearance of spin splitting requires first the violation of  $\theta I$  symmetry. In magnetic crystals, where  $\theta$  is already violated due to magnetic order, absence of the inversion  $I$  symmetry doesn’t mean breaking of  $\theta I$ , hence does not necessarily lead to the removal of spin degeneracy. (Actually, even for a *centrosymmetric* magnetic structure, where  $I$  is preserved but  $\theta I$  is broken, one can still have spin splitting). (ii) To have SOC-unrelated spin splitting, one needs also to violate  $UT$  symmetry. AFM structures that violate  $UT$  symmetry correspond to the so-called MSG type III or I such as rutile  $\text{MnF}_2$ . Supplementary section II provides more detailed discussion of  $UT$  symmetries.

**TABLE I | Classification of four spin splitting prototypes in antiferromagnetic compounds in terms of symmetry conditions, consequences, and examples.** *Symmetry conditions:*  $\theta$  represents time reversal and  $I$  represents spatial inversion,  $\theta I$  is the combination of these two operations. AFM can be MSG type I, III or IV. (For detail description of MSG and MSG type please refer to supplementary section II). *Consequences:* No SS means no spin splitting either with or without SOC. SOC- induced SS means that one has spin splitting when SOC is non-zero, but no spin splitting when SOC is turned off. AFM induced SS means that one has spin splitting even when SOC is

turned off. Note that the symmetry-based conditions generally apply not only to collinear but also to noncollinear AFM. For example, we would expect AFM-induced spin splitting in a non-collinear AFM  $\text{Mn}_3\text{Ir}$ <sup>27</sup> which is also centrosymmetric but has no  $\theta I$  symmetry and belongs to MSG type III.

AFM SS PROTOTYPE	1	2	3	4
CONDITION 1: HAS $\theta I$ ?	Yes	Yes	No	No
CONDITION 2: MSG TYPE	III	IV	IV	I OR III
CONSEQUENCES	No SS	No SS	SOC Induced SS	AFM induced SS
EXAMPLES	$\text{CuMnAs}$ <sup>28</sup>	$\text{NiO}$ <sup>29</sup>	$\text{BiCoO}_3$ <sup>30</sup>	$\text{MnF}_2$ <sup>31</sup>

**Prototypes of AFM SS:** Based on whether the AFM compound in question has or lacks  $\theta I$  symmetry, and whether it belongs to MSG type IV or MSG type I / III, we have identified four distinct types of AFM spin splitting prototypes (Table I). The first two prototypes, (1) (2), have spin degeneracy at arbitrary  $k$  point because of protection by  $\theta I$  symmetry. The prototypes (3) (4) have  $\theta I$  violation, allowing spin splitting in the presence of SOC. Prototype (3) being MSG type IV has spin degeneracy when SOC is turned off (referred as “SOC induced spin splitting”) whereas prototype (4) being MSG type I or III allows spin splitting even when SOC is turned off (referred as “AFM induced spin splitting”). To find specific compound realizations of the four AFM prototypes (last line of Table I) one can search listings of magnetic symmetries (such as the Bilbao listing<sup>32</sup>) for compliance with our design principles (top 2 lines in Table I). As a concrete example, we illustrate the identification of a realization of AFM SS prototype 4 compound. Tetragonal  $\text{MnF}_2$  having magnetic space group  $P4_2'/\text{mnm}'$  complies with the above noted design principles -- (1) has no  $\theta I$  symmetry despite the presence of inversion symmetry; (2) belongs to MSG type III, therefore no  $UT$  symmetry.

Table I indicates that not all AFM compounds have the same SS behavior, and that the magnetic, not just spatial symmetries are important. For example, an AFM SS has been theoretically analyzed recently based on tight-binding models on the multipole description by Hayami et. al.<sup>33,34</sup>. However, their multipole analysis was based on point group symmetry not magnetic group symmetry, omitted the non-magnetic atoms. This omission (e.g.  $\text{MnF}_2$  without F), however, restores the  $UT$  symmetry and results in the prediction of complete spin degeneracy in the absence of SOC, in sharp contrast with DFT predicted (below) giant spin splitting. (see supplementary section I for detail discussion of these previous work)

**Illustration of the properties of a AFM-induced SS compound  $\text{MnF}_2$ :**  $\text{MnF}_2$  is a wide gap insulator both below and above its Néel temperature of 67K.<sup>35</sup> It is a centrosymmetric rutile structure (conventional space group  $P4_2/\text{mnm}$ ), with magnetic Mn ions occupying position (0, 0, 0) and (1/2, 1/2, 1/2) centered in an octahedral of non-magnetic F anions located at  $\pm(u, u, 0)$  and  $\pm(1/2+u, 1/2-u, 1/2)$  where  $u$  is the positional parameter. The refinement X-ray diffraction results<sup>36</sup> gave the positional

parameter  $u=0.305$ , and lattice constant  $a=b=4.873$  Å,  $c=3.311$  Å. Erickson<sup>31</sup> found via neutron scattering measurements the AFM moment aligned along the tetragonal axis (i.e., [001]) with magnetic space group of  $P4_2'/mmn'$ . The magnetic crystal unit cell is shown in Figure 1(a). While concentrating on this specific material  $MnF_2$  as an illustration of a new physical effect, we do not maintain that it is optimized for technological usage in a specific spintronics device application (size of band gap; dopability; value of Néel temperature) optimization of such material constants might be possible by comparing different compounds belonging to a given AFM SS prototype. This is outside the scope of the current paper.

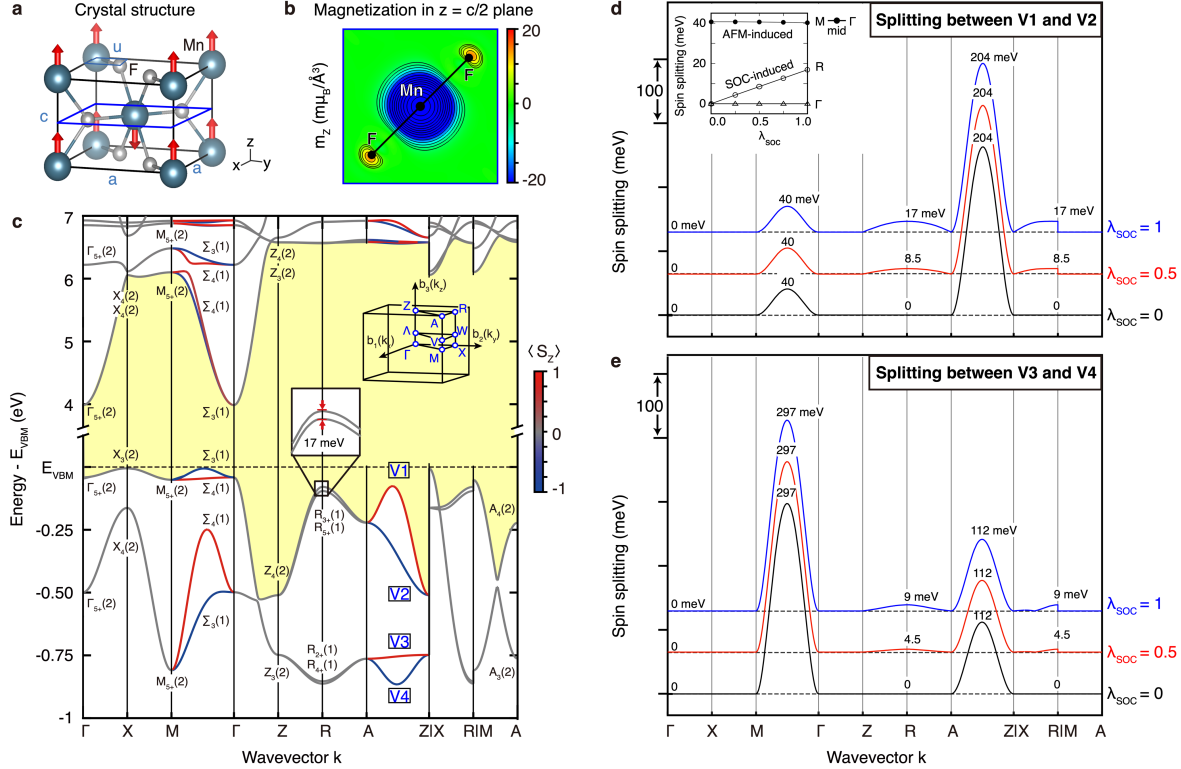


**Figure 1 | Crystal structure, band structure and spin splitting in centrosymmetric AFM tetragonal  $MnF_2$ .** (a) Magnetic unit cell where red arrows indicate local magnetic moment; (b) contour plot of magnetization along  $z$  in  $z = c/2$  plane; (c) DFT calculated band structure with our calculated magnetic symmetry representations (see supplementary section III), using the notations of Ref. <sup>37</sup> with numbers in parenthesis indicating the dimension of the representation (i.e., degeneracies). The top four valence bands are denoted by V1, V2, V3, V4 and the yellow screen highlights the gaps between valence and conduction bands. Insert of (c) shows the BZ and the blow-up bands around R point. The blue to red color scale denotes calculated out-of-plane spin polarization. Panels (d, e) show DFT calculated wave vector dependence of the spin splitting between pairs of valence bands V1-V2 (in (d)) and between V3-V4 (in (e)) for different scaling of SOC  $\lambda_{SOC}$  (numerical coefficient  $0 < \lambda_{SOC} < 1$ ). Insert of (d) shows the spin splitting vs. the amplitude of the spin orbit coupling  $\lambda_{SOC}$  at  $\Gamma$  (0, 0, 0), R (0, 0.5, 0.5) and the middle point of  $\Gamma$ -M (0.25, 0.25, 0). All DFT calculations use PBE exchange correlation functional<sup>38</sup> with on-site coulomb interaction on Mn-3d orbitals of  $U=5$  eV,  $J=0$  eV and the experimental crystal structure<sup>36</sup>.

**DFT validation of SS characteristics in MnF<sub>2</sub>:** We calculated the relativistic electronic structure of AFM MnF<sub>2</sub> within density functional theory (DFT) (see description of DFT method in supplementary section III). Figure 1(b) provides the calculated magnetization  $m_z(\mathbf{r}) = m^\uparrow(\mathbf{r}) - m^\downarrow(\mathbf{r})$  in the  $c=z/2$  plane, with  $m^\uparrow$  and  $m^\downarrow(\mathbf{r})$  representing the up and down spin electron density. To assess the AFM magnetism effect we also define a reference NM model, where the magnetic moment on each site is zero, resulting in a metallic state. We emphasize that the NM model is not used to mimic the physical high temperature paramagnetic (PM) phase that has a distribution of non-vanishing local magnetic moments that creates an insulating gap even in the absence of long-range order.<sup>39,40</sup> Figure 1(c) gives the band structure of the AFM phase calculated with SOC in its experimental crystal structure. We find a  $z$  oriented magnetic moment on Mn<sup>2+</sup> of  $4.7 \mu_B$ , in good agreement with the neutron scattering measurement of  $4.6 \mu_B$ . We also find calculated minimum direct gap at  $\Gamma$  of 4.02 eV and a smaller indirect gap between VBM at X and CBM at  $\Gamma$  of 3.98 eV, comparable with the measured absorption gap<sup>41</sup> of 4.1 eV (estimated from the convergence limit of the observed series of discrete d-d\* multiplet transitions into the onset of band-to-band continuum). The DFT (mean field) calculated band gap and DFT local moment both agree with experiment, providing strong evidence that the single-particle band structure picture with a 5 eV wide band width as advanced in the DFT calculations holds well, supporting the notion of well-defined coherent bands.

To assist future measurements of the predicted AFM-induced  $\mathbf{k}$ -dependent spin splitting (e.g. via ARPES and spin-ARPES) as well as potential applications in novel spintronics we next describe the main predicted features of the AFM-induced spin splitting:

(i) *The spin splitting has a typical atomic-like energy scale (“giant splitting”):* Despite rather small atomic numbers in MnF<sub>2</sub> ( $Z(\text{Mn})=25$  and  $Z(\text{F})=9$ ), the magnitude of the spin splitting (up to 300 meV seen between V3 and V4 along  $\Gamma$ -M in Figure 1(e)) arising from the AFM mechanism can be comparable to some of the largest known spin splitting of conventional electric mechanism for heavy atom high  $Z$  compounds, such as the ‘giant SOC’ induced spin splitting in BiTeI<sup>42</sup> and GeTe<sup>43,44</sup>. The reason for the difference is that the magnetic field which induces the splitting in AFM reflects the local magnetic moments *localized about atomic sites*, not as in the SOC effect where the inducing magnetic field reflects the asymmetry in the *inter-atomic regions* of the unit cell. The locality of magnetic moments needed for obtaining large spin splitting does not contradict the requirement to introduce itinerant carriers. Local magnetic moments of  $4\text{-}5 \mu_B$  are common in Mn-salts with broad (4-5 eV) bands and high electronic mobility, e.g., La<sub>1-x</sub>Sr<sub>x</sub>MnO<sub>3</sub><sup>45</sup>. We find that the spin split bands in MnF<sub>2</sub> occur about 40 meV below the VBM (bands V1-V2 in Figure 1) and about 500 meV below the VBM (bands V3-V4 in Figure 1). Either should be amenable to photoemission detection for validating the theory.

(ii) *The splitting persists even if SOC=0:* The spin splitting along the  $\Gamma$ -M and Z-A lines is present even when SOC is turned off in the Hamiltonian (black line in Figure 1(d) and (e); also shown in the insert of (d)). This is very different from type 3 AFM (Table I) BiCoO<sub>3</sub><sup>23</sup>, where spin splitting disappears if SOC vanishes. Thus, the AFM-induced spin splitting mechanism delivers the long-standing hope for wave vector dependent spin splitting mechanism in thermodynamically stable, low  $Z$  compounds.

(iii) *Relative to the NM case, AFM induces a highly anisotropic and  $\mathbf{k}$ -dependent spin splitting:* We show in Figure 2 the band structures of centrosymmetric  $\text{MnF}_2$  in two cases (a) NM without SOC; (b) AFM without SOC. In both cases we indicate the degeneracies of states, calculated by DFT shown as integer values. An important manifestation of the AFM- induced spin splitting (Figure 1(c)) is that whereas in the NM structure, the whole BZ, including directions  $\Gamma$ -X and  $\Gamma$ -M, have double degenerate (non-split) bands, in the AFM structure spin splitting arises even in the absence of SOC but it is wave vector dependent. Bands remain degenerate along the  $\Gamma$ -X directions, but become spin split along the  $\Gamma$ -M direction. Such anisotropic spin splitting was already hinted by the asymmetry in magnetization in coordinate space as shown in Figure 1(b) between  $x + y$ ,  $x - y$  and  $x$ ,  $y$  directions. This behavior is understandable on the basis of magnetic symmetry (See supplementary IV for discussion of unitary and antiunitary symmetries): the AFM ordering does not lead to symmetry reduction along the  $\Gamma$ -X paths, relative to its NM counterpart. The resulting spin degeneracy along  $k_x$  (or  $k_y$ ) direction of  $\Gamma$ -X in AFM is protected by its group of  $\mathbf{k}$  symmetries  $\theta\{C_{2x}|\tau\}$  and  $\theta\{\sigma_{vy}|\tau\}$  (or  $\theta\{C_{2y}|\tau\}$  and  $\theta\{\sigma_{vx}|\tau\}$ ). In contrast, along the  $\Gamma$ -M paths, in AFM the combined symmetries of  $\theta\{C_{2a}|0\}$  and  $\theta\{C_{2b}|0\}$  (or  $\theta\{\sigma_{da}|0\}$  and  $\theta\{\sigma_{db}|0\}$ ) are broken, which creates spin splitting. Here,  $C_{2x}$ ,  $C_{2y}$ ,  $C_{2a}$ ,  $C_{2b}$  are  $\pi$  rotations about the [100], [010], [110], [1-10] axes, respectively;  $\sigma_{vx}$ ,  $\sigma_{vy}$ ,  $\sigma_{da}$ ,  $\sigma_{db}$  are mirror reflections in (100), (010), (1-10), (110) planes; and vector  $\tau = (1/2, 1/2, 1/2)$  is half lattice translation, directed along the spatial diagonal [111] of the unit cell. Similar arguments (given in Supplementary section IV) apply for spin degeneracy along Z-R and spin splitting along Z-A in Figure 1(b).

(iv) *The AFM mechanism gives rise to even powers of  $k$  in the spin splitting:* Of special interest in Figure 1 (c) is the diagonal  $\Gamma$ -M and Z-A line showing large spin splitting while at the end of these  $\mathbf{k}$ -lines the splitting vanishes. It is of interest therefore, to establish how the splitting changes near its  $\mathbf{k}$ -space end points. By fitting the DFT calculated spin splitting  $\Delta_{ss}(\mathbf{k})$  to the power of  $k$ , we found a quadratic-in- $k$  dependence at  $\Gamma$ -M and  $M$ - $\Gamma$  (see details of fitting in supplementary section V and effective model in supplementary section VI). Thus, near degeneracy points  $\Delta_{ss}(\mathbf{k})$  has a quadratic  $k$  dependence compared with odd powers typical of the electrically induced SOC effect.

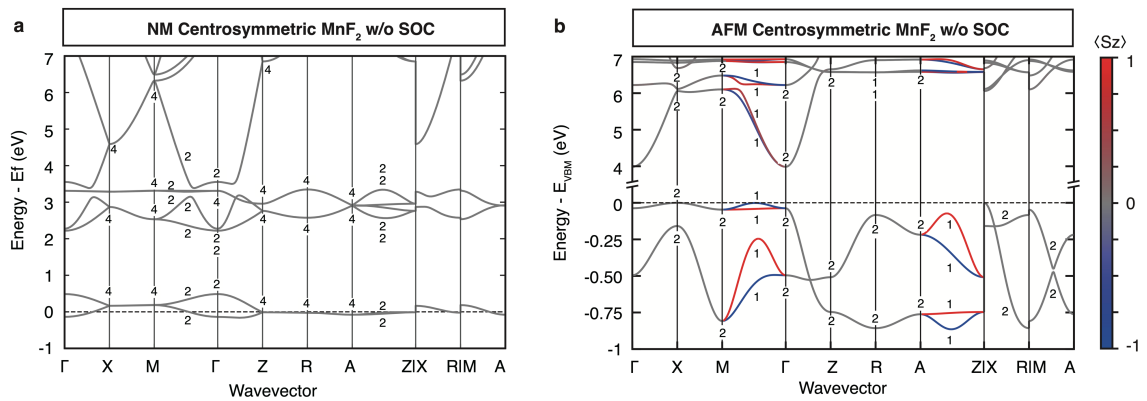


**Figure 2 | DFT band structures of Centrosymmetric (CS)  $\text{MnF}_2$  in NM and AFM without SOC.** In all cases we use the experimentally observed centrosymmetric tetragonal structure<sup>36</sup>: (a) NM with SOC set to

zero; **(b)** AFM with SOC set to zero. Out-of-plane spin polarizations are mapped to color scales from blue to red. The integer number attached to each band and  $\mathbf{k}$  point is degeneracies.

(v) A Dresselhaus in-plane spin texture results from a cooperative SOC and AFM effect: The coupling between spin space and position space results not only in spin-splitting of the energy spectrum, but also in developing “spin-momentum locking”, where the spin orientation is locked with momentum  $\mathbf{k}$ . The vector field of the spin states in momentum space is called spin texture, being helical for the conventional Rashba SOC mechanism<sup>3</sup> and non-helical for the Dresselhaus mechanism<sup>2</sup>. The spin texture for AFM-induced spin splitting has its own fingerprints. Figure 3 shows the calculated spin texture of the V1 and V2 bands at the representative  $\mathbf{k}$ -plane  $k_z = \pi/2c$  where  $c$  is the lattice constant along  $z$  axis. We see that, electron spins are mostly aligned along the out-of-plane  $z$  direction, as can be surmised from the magnetic structure (see Figure 1(a)). This is seen in the four quadrants patterns on a fixed  $k_z$  plane with positive (up arrow in Figure 3(a) and (b)) and negative (down arrow in Figure 3(a) and (b)) out-of-plane spin polarization in the neighbor quadrants. The out-of-plane spin polarizations are opposite in sign between bands V1 and V2, as noted by the reversal of the red and blue patterns for V1 and V2. Similar four quadrants pattern of out-of-plane spin polarization is also found in the  $k_z = 0$  and  $k_z = \pi/c$  planes (see corresponding spin texture results in Supplementary section VII).

Interestingly, inspecting the  $k_z = \pi/2c$  plane, Figure 3 shows a pronounced (i) in-plane (ii) non-helical Dresselhaus-like spin texture. These features are unexpected given that the crystal structure of  $\text{MnF}_2$  is magnetized in the  $z$ -direction and centrosymmetric, while normally to assure Dresselhaus features<sup>4</sup> we need non-centrosymmetric symmetry. We find that the Dresselhaus spin texture in  $\text{MnF}_2$  requires for its existence the SOC term (i.e. the texture vanishes if the SOC is removed from the Hamiltonian). Thus, the texture represents the combined effect of coexistence of SOC with AFM (see cooperative effect on spin splitting in Supplementary section VIII).

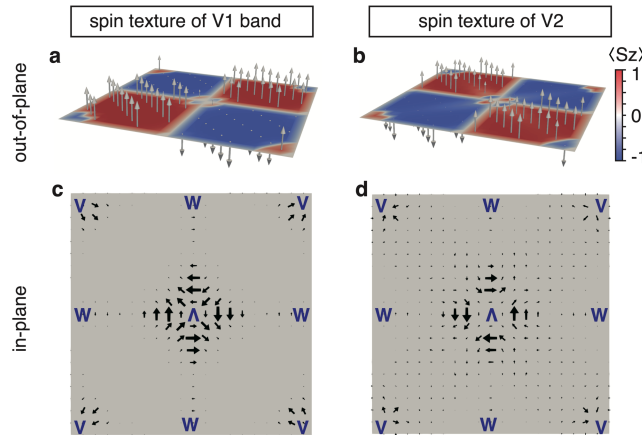


**Figure 3 | Spin texture in AFM  $\text{MnF}_2$  with SOC on  $k_z = \pi/2c$  plane. (a)** Out-of-plane spin texture of V1 band, **(b)** out-of-plane spin texture of V2 band, **(c)** in-plane spin texture of V1 band, and **(d)** in-plane spin texture of V2 band.



(vi) *Different wavevectors can have different dependence on SOC strength:* The insert of Figure 1(d) shows different characteristic behaviors of the dependence of spin splitting  $\Delta_{ss}(\mathbf{k})$  on spin-orbit strength at different  $\mathbf{k}$  points: (1) The trivial case (e.g.  $\Gamma$  point) is that neither magnetic nor SOC induces any splitting; (2) the R point shows zero spin splitting when  $\lambda_{SOC} = 0$  and linear dependence of  $\lambda_{SOC}$ , illustrating a cooperation of both magnetic and SOC mechanism; notice that despite R being a TRIM point, it shows spin splitting, unlike the case of purely SOC induced effects; (3) the non-trivial case of purely magnetic induced spin splitting occurs along  $\Gamma$ -M (as well as A-Z) line, where non-zero spin splitting is present even at  $\lambda_{SOC} = 0$  and is almost independent of  $\lambda_{SOC}$ . The appearance of such distinct spin splitting behaviors at different wave vectors in a single compound would be advocated for multifunctional spintronic applications.

## DISCUSSION

This study uncovers the design principles of spin splitting in AFM compounds based on magnetic symmetry analysis and shows a very rich set of fingerprint fundamental physical effects ((i)-(vi) above) in a specific prototype, including the giant spin splitting that characterizes the AFM mechanism and could aid its future experimental observation. The present symmetry-based theory with atomistic resolution enabled by DFT instills content into the 1964 phenomenological theory by Pekar and Rashba<sup>1</sup> proposing a pioneering magnetic spin splitting mechanism.

The mechanism described here foresees many encouraging physical phenomena. As an example, active research is going currently on 2D layered systems consisting of two layers, of which one is an AFM and the other a heavy metal such as Pt, with the SOC of Rashba-type developing on their interface and controlled by electric bias applied across it.<sup>46 47</sup> Using antiferromagnets with spin-split bands, which in addition are either magneto-electric or piezoelectric, might eliminate necessity of the heavy-metal layer due to the giant magnitude of spin-orbit splitting found above. We also note a few transport effects that are likely associated to the AFM-induced spin splitting effect. These include finite spin current predicted by Yan et. al.<sup>48</sup>, anomalous hall conductivity predicted by MacDonald et. al.<sup>49</sup> and Arita et. al.<sup>50</sup> and crystal hall effect proposed<sup>51</sup> and verified<sup>52</sup> by Jungwirth and Sinova et. al.

**Data availability.** The data that support the findings of this study are available from the corresponding author upon reasonable request.

**Acknowledgment.** The National Science Foundation (NSF) Grant NSF-DMR-CMMT No DMR-1724791 supported the theory development of this work by L.-D.Y., Z.W., and A.Z. at the University of Colorado Boulder. The *ab initio* calculations of this work were supported by the U.S. Department of Energy, Office of Science, Basic Energy Sciences, Materials Sciences and Engineering Division under Grant No. DE-SC0010467. J.-W. L. was supported by the National Natural Science Foundation of China (NSFC) under Grant Number 61888102. This work used resources of the National Energy Research Scientific Computing Center, which is supported by the Office of Science of the U.S. Department of Energy under Contract No. DE-AC02-05CH11231. We thank Dr. Carlos Mera Acosta for fruitful discussions.

**Author contribution.** AZ and ER conceived and directed the study. LDY did the majority of the computational work and analysis; ZW participated in the computation and numerical method development; JWL contributed to the writing and discussions; AZ directed the analysis and wrote the text with input from all authors.

**Competing interests.** The authors declare no competing interests.

**Correspondence and requests for materials** should be addressed to A.Z.

## REFERENCES

- 1 Pekar, S. I. & Rashba, E. I. Combined resonance in crystals in inhomogeneous magnetic fields. *Zh. Eksperim. i Teor. Fiz.* **47**, (1964), English translation: Sov. Phys. - JETP **20**, 1295 (1965).
- 2 Dresselhaus, G. Spin-Orbit Coupling Effects in Zinc Blende Structures. *Physical Review* **100**, 580-586, (1955).
- 3 Rashba, E. & Sheka, V. Symmetry of energy bands in crystals of wurtzite type II. Symmetry of bands with spin-orbit interaction included. *Fiz. Tverd. Tela, Collected Papers (Leningrad)* **2**, (1959), English translation: [https://iopscience.iop.org/1367-2630/17/5/050202/media/njp050202\\_suppdata.pdf](https://iopscience.iop.org/1367-2630/17/5/050202/media/njp050202_suppdata.pdf).
- 4 Zhang, X., Liu, Q., Luo, J.-W., Freeman, A. J. & Zunger, A. Hidden spin polarization in inversion-symmetric bulk crystals. *Nature Physics* **10**, 387-393, (2014).
- 5 Landau, L. D. *et al.* *Electrodynamics of continuous media*. Vol. 8 (Oxford, Butterworth-Heinemann) (1989).
- 6 Wolf, S. A. *et al.* Spintronics: A Spin-Based Electronics Vision for the Future. *Science* **294**, 1488-1495, (2001).
- 7 Žutić, I., Fabian, J. & Sarma, S. D. Spintronics: Fundamentals and applications. *Rev Mod Phys* **76**, 323-410, (2004).
- 8 Fert, A. The present and the future of spintronics. *Thin Solid Films* **517**, 2-5, (2008).
- 9 Manchon, A., Koo, H. C., Nitta, J., Frolov, S. M. & Duine, R. A. New perspectives for Rashba spin-orbit coupling. *Nat Mater* **14**, 871-882, (2015).
- 10 Harrison, W. *Electronic Structure and the Properties of Solids*, 1980. *WH Freeman and Co., San Francisco*, (1989).
- 11 Taguchi, T. & Ray, B. Point defects in II–VI compounds. *Prog Cryst Growth Charact* **6**, 103-162, (1983).
- 12 West, D., Sun, Y. Y., Wang, H., Bang, J. & Zhang, S. B. Native defects in second-generation topological insulators: Effect of spin-orbit interaction on Bi<sub>2</sub>Se<sub>3</sub>. *Physical Review B* **86**, 121201, (2012).
- 13 Edwards, A. *et al.* Electronic structure of intrinsic defects in crystalline germanium telluride. *Physical Review B* **73**, 045210, (2006).
- 14 Bailly, F. Energies of Formation of Metal Vacancies in II-VI Semiconducting Tellurides (HgTe, CdTe, ZnTe). *Physica Status Solidi (b)* **25**, 317-322, (1968).
- 15 Sánchez, J. C. R. *et al.* Spin-to-charge conversion using Rashba coupling at the interface between non-magnetic materials. *Nature communications* **4**, 2944, (2013).
- 16 Baltz, V. *et al.* Antiferromagnetic spintronics. *Reviews of Modern Physics* **90**, 015005, (2018).
- 17 Jungwirth, T., Marti, X., Wadley, P. & Wunderlich, J. Antiferromagnetic spintronics. *Nat Nanotechnol* **11**, 231-241, (2016).

- 18 MacDonald, A. H. & Tsoi, M. Antiferromagnetic metal spintronics. *Philosophical Transactions Royal Soc Math Phys Eng Sci* **369**, 3098-3114, (2011).
- 19 Manchon, A. *et al.* Current-induced spin-orbit torques in ferromagnetic and antiferromagnetic systems. *1801.09636* **91**, 035004, (2019).
- 20 Gao, G. Y. & Yao, K.-L. Antiferromagnetic half-metals, gapless half-metals, and spin gapless semiconductors: The D0 3 -type Heusler alloys. *Applied Physics Letters* **103**, 232409, (2013).
- 21 Gong, S.-J. *et al.* Electrically induced 2D half-metallic antiferromagnets and spin field effect transistors. *Proceedings of the National Academy of Sciences* **115**, 8511-8516, (2018).
- 22 Hu, S.-J. & Hu, X. Half-Metallic Antiferromagnet BaCrFeAs 2. *J Phys Chem C* **114**, 11614-11617, (2010).
- 23 Yamauchi, K., Barone, P. & Picozzi, S. Bulk Rashba effect in multiferroics: A theoretical prediction for BiCoO<sub>3</sub>. *Physical Review B* **100**, 245115, (2019).
- 24 Ramazashvili, R. Kramers Degeneracy in a Magnetic Field and Zeeman Spin-Orbit Coupling in Antiferromagnetic Conductors. *Physical Review Letters* **101**, 137202, (2008).
- 25 Rozbicki, E. J., Annett, J. F., Souquet, J.-R. & Mackenzie, A. P. Spin-orbit coupling and k-dependent Zeeman splitting in strontium ruthenate. *Journal of Physics: Condensed Matter* **23**, 094201, (2011).
- 26 Tang, P., Zhou, Q., Xu, G. & Zhang, S.-C. Dirac fermions in an antiferromagnetic semimetal. *1603.08060* **12**, 1100-1104, (2016).
- 27 Tomeno, I., Fuke, H. N., Iwasaki, H., Sahashi, M. & Tsunoda, Y. Magnetic neutron scattering study of ordered Mn<sub>3</sub>Ir. *Journal of Applied Physics* **86**, 3853-3856, (1999).
- 28 Wadley, P. *et al.* Antiferromagnetic structure in tetragonal CuMnAs thin films. *Scientific reports* **5**, 17079, (2015).
- 29 Ressouche, E., Kernavanois, N., Regnault, L.-P. & Henry, J.-Y. Magnetic structures of the metal monoxides NiO and CoO re-investigated by spherical neutron polarimetry. *Phys B Condens Matter* **385**, 394-397, (2006).
- 30 Belik, A. A. *et al.* Neutron Powder Diffraction Study on the Crystal and Magnetic Structures of BiCoO<sub>3</sub>. *Chemistry of Materials* **18**, 798-803, (2006).
- 31 Erickson, R. A. Neutron Diffraction Studies of Antiferromagnetism in Manganous Fluoride and Some Isomorphous Compounds. *Physical Review* **90**, 779-785, (1953).
- 32 Gallego, S. V. *et al.* MAGNDATA : towards a database of magnetic structures. I. The commensurate case. *J Appl Crystallogr* **49**, 1750-1776, (2016).
- 33 Hayami, S., Yanagi, Y. & Kusunose, H. Momentum-Dependent Spin Splitting by Collinear Antiferromagnetic Ordering. *J Phys Soc Jpn* **88**, 123702, (2019).
- 34 Naka, M. *et al.* Spin current generation in organic antiferromagnets. *Nature communications* **10**, 4305, (2019).
- 35 Stout, J. W. & Adams, H. E. Magnetism and the Third Law of Thermodynamics. The Heat Capacity of Manganous Fluoride from 13 to 320°K. *Journal of the American Chemical Society* **64**, 1535-1538, (1942).
- 36 Baur, W. H. & Khan, A. A. Rutile-type compounds. IV. SiO<sub>2</sub>, GeO<sub>2</sub> and a comparison with other rutile-type structures. *Acta Crystallogr Sect B Struct Crystallogr Cryst Chem* **27**, 2133--2139, (1971).
- 37 Dimmock, J. O. & Wheeler, R. G. Symmetry Properties of Wave Functions in Magnetic Crystals. *Physical Review* **127**, 391-404, (1962).
- 38 Perdew, J. P. *et al.* Atoms, molecules, solids, and surfaces: Applications of the generalized gradient approximation for exchange and correlation. *Physical Review B* **46**, 6671, (1992).
- 39 Varignon, J., Bibes, M. & Zunger, A. Origin of band gaps in 3d perovskite oxides. *Nature communications* **10**, 1658, (2019).

- 40 Trimarchi, G., Wang, Z. & Zunger, A. Polymorphous band structure model of gapping in the antiferromagnetic and paramagnetic phases of the Mott insulators MnO, FeO, CoO, and NiO. *Physical Review B* **97**, 035107, (2018).
- 41 Stout, J. W. Absorption Spectrum of Manganous Fluoride. *J Chem Phys* **31**, 709-719, (1959).
- 42 Ishizaka, K. *et al.* Giant Rashba-type spin splitting in bulk BiTeI. *Nat Mater* **10**, 521-526, (2011).
- 43 Sante, D. D., Barone, P., Bertacco, R. & Picozzi, S. Electric Control of the Giant Rashba Effect in Bulk GeTe. *Advanced materials* **25**, 509-513, (2012).
- 44 Liebmann, M. *et al.* Giant Rashba-Type Spin Splitting in Ferroelectric GeTe(111). *Advanced materials* **28**, 560-565, (2015).
- 45 May, S. J. *et al.* Enhanced ordering temperatures in antiferromagnetic manganite superlattices. *Nature Materials* **8**, 892-897, (2009).
- 46 Železný, J. *et al.* Relativistic Néel-Order Fields Induced by Electrical Current in Antiferromagnets. *Physical Review Letters* **113**, 157201, (2014).
- 47 Wadley, P. *et al.* Electrical switching of an antiferromagnet. *Science* **351**, 587, (2016).
- 48 Železný, J., Zhang, Y., Felser, C. & Yan, B. Spin-Polarized Current in Noncollinear Antiferromagnets. *Physical Review Letters* **119**, 187204, (2017).
- 49 Chen, H., Niu, Q. & MacDonald, A. H. Anomalous Hall Effect Arising from Noncollinear Antiferromagnetism. *Physical Review Letters* **112**, 017205, (2014).
- 50 Suzuki, M. T., Koretsune, T., Ochi, M. & Arita, R. Cluster multipole theory for anomalous Hall effect in antiferromagnets. *Physical Review B* **95**, 094406, (2017).
- 51 Šmejkal, L., González-Hernández, R., Jungwirth, T. & Sinova, J. Crystal Hall effect in Collinear Antiferromagnets. *Preprint at <https://arxiv.org/abs/1901.00445>*, (2019).
- 52 Feng, Z. *et al.* Observation of the Crystal Hall Effect in a Collinear Antiferromagnet. *Preprint at <https://arxiv.org/abs/2002.08712>*, (2020).